Archives of Civil and Mechanical Engineering (2020) 20:46
https://doi.org/10.1007/s43452-020-00048-8

ORIGINAL ARTICLE

Spacing and bundling effects on rate-dependent pullout behavior of various steel fibers embedded in ultra-high-performance concrete

Jae-Jin Kim[1] · Doo-Yeol Yoo[2]

Received: 9 February 2020 / Revised: 23 March 2020 / Accepted: 25 March 2020 / Published online: 6 April 2020

Abstract
This study examines the effects of fiber geometry, spacing, and loading rate on the pullout resistance of steel fibers in ultra-high-performance concrete (UHPC). For this, three different types of steel fibers, four different fiber spacings, and three different loading rates ranging from 0.018 to 740 mm/s were considered. Test results indicated that the single straight fiber in UHPC was most rate sensitive for pullout resistance, followed by the single twisted and then hooked fibers. The bond strengths and pullout energy of specimens with multiple straight fibers were improved by increasing the loading rate but were not affected by fiber spacing. Closer fiber spacing had a detrimental effect on the dynamic pullout resistance of multiple hooked steel fibers in UHPC, while no enhancement of average bond strength of multiple twisted fibers was observed as fiber spacing and loading rate varied. The average bond strengths of single and bundled hooked and twisted steel fibers in UHPC were clearly improved by increasing the loading rate. Bundling of fibers enhanced the impact pullout resistance of all the steel fibers in UHPC. The highest dynamic increase factors for the bundled straight, hooked, and twisted fibers were approximately 3.78, 1.57, and 1.41, respectively, at the impact loads.

Keywords Ultra-high-performance concrete · Steel fibers · Pullout resistance · Fiber spacing · Fiber bundling effect · Rate sensitivity

1 Introduction

Ultra-high-performance concrete (UHPC) was first introduced in the mid-1990s in research performed by Richard and Cheyrezy [1] concerning reactive powder concrete. A UHPC generally exhibits high durability [2, 3] and is characterized by significantly higher compressive strength than conventional concrete, with maximization of particle packing density by the use of fine aggregates. However, due to the high compressive strength, UHPC is extremely brittle because of rapid dissipation of a large amount of energy in failure mode [4]. It is necessary to ensure a strain- or deflection-hardening behavior with sufficient energy absorption capacity that can be achieved through improvement in post-cracking tensile behavior from fiber bridging at the crack surface by incorporating various discontinuous fibers. Due to the excellent bridging capability of fibers in UHPC, multiple microcracks are formed in the hardening zone, delaying failure and leading to stress redistribution after initial matrix cracking [5, 6]. Yoo et al. [5] observed the deflection-hardening behavior of UHPC containing straight steel fibers with a formation of multiple microcracks. At crack plane, the tensile force is mainly resisted by the bridging fibers and transmitted to the surrounding matrix. Once the transmitted tensile stress exceeds the tensile strength of matrix, another crack is newly formed, which is a mechanism of multiple crack formation. Graybeal and Baby [6] also noted that fibers resist microcracking behavior in the strain-hardening zone, broadening the stress redistribution area. These composites with added fibers are called ultra-high-performance fiber-reinforced concrete (UHPFRC), studied and used in many countries in recent years [7–10]. For UHPFRC to meet the requirements of international codes, e.g., Association

✉ Doo-Yeol Yoo
dyyoo@hanyang.ac.kr

Jae-Jin Kim
redgoblue@hanyang.ac.kr

[1] Department of Architectural Engineering, Hanyang University, 222 Wangsimni-ro, Seongdong-gu, Seoul 133-791, Republic of Korea

[2] Department of Architectural Engineering, Hanyang University, 222 Wangsimni-ro, Seongdong-gu, Seoul 04763, Republic of Korea

Française de Génie Civil (AFGC) and American Concrete Institute (ACI) [7, 8], it must exhibit very high compressive strength of over 150 MPa and tensile strength of 8 MPa.

Bond properties between the fiber and cement matrix play a highly influential role in determining the mechanical performance of UHPFRC [11]. Some important properties determining the quality of the bond are the fiber embedment length, orientation, type, loading rate, matrix properties, etc. Several researchers [12–19] have studied fiber pullout behaviors of UHPC under various conditions. Studies on steel fiber pullout behavior in UHPC have been conducted generally in a quasi-static loading condition through single-fiber pullout tests [13, 14], while relatively few studies analyzing the dynamic pullout behavior of the single fiber are available [15, 16]. Wille and Naaman [13] reported that deformed steel fiber in a single-fiber pullout test exhibited an equivalent bond strength about five times greater than that of a straight steel fiber in a UHPC matrix under the same conditions. In addition, they [13, 14] noted that bond properties between steel fibers and matrix can be enhanced by increasing particle packing. Tai et al. [15, 16] examined pullout behaviors of three differently shaped steel fibers (straight, hooked, and twisted) in UHPC, with varying inclination angles (ranging 0°–45°) and loading rates (ranging 0.018–1800 mm/s). In their study, straight steel fibers exhibited a dynamic increase factor (DIF) of 2.32 under impact loads and were most sensitive to the loading rates. The DIFs of deformed steel fibers were lower than those of straight fibers, and the DIF of twisted fibers at high inclined angles dropped below 1. Lee et al. [12] examined the pullout behavior of inclined steel fibers in UHPC and found that the largest fiber pullout load was obtained at inclination angles of 30° or 45°, and the slip at peak load increased as the inclined angle increased. Yoo et al. [17] examined the pullout behavior of steel fibers in cement matrices of varying compressive strengths (ranging 112.2–190.2 MPa) and reported that fiber pullout resistance improved as matrix strength increased. Chun and Yoo [18] investigated the effects of hybrid use of macro and micro steel fibers in UHPC on fiber pullout and tensile behaviors of composites. They found that, by replacing macro fibers with micro straight steel fibers, the average bond strength and the normalized pullout energy increased in straight steel fibers but decreased in deformed fibers.

However, while fiber pullout test results can provide important information concerning the post-cracking tensile behavior of UHPFRC, it is difficult to identify a strong correlation between pullout and tensile behaviors. To be specific, Yoo et al. [17] reported, in the deformed fibers, the correlation between flexural behavior of composites and pullout response of single fibers was low. Similarly, Chun and Yoo [18] noted no correlation between fiber pullout behavior and tensile behavior of composites in their experiment. Opposing results have been obtained since some conditions are not able to be realized in the fiber pullout test, such as effects of adjacent fibers, fiber random distribution, and volume of matrix surrounding the fibers. Steel fiber content in UHPFRC is one of the important factors directly affecting these conditions. As fiber spacing is reduced, there will be an increase in the probabilities of being influenced by adjacent fibers and form fiber balls or fiber bundling. These phenomena make it difficult to predict the performance of fibers in reinforcing the cement matrix and even deteriorate the tensile performance of UHFPRC in some cases, so the effect of adjacent fibers on the pullout response needs to be investigated. Although there are some studies that have analyzed multiple fibers in UHPC [12, 18], they did not examine the effect of fiber spacing on the pullout behavior of multiple steel fibers in UHPC. Recently, an experiment for investigating the effects of fiber type and spacing on pullout behavior under static conditions was performed by Kim and Yoo [19]. They reported several important findings: (1) The average bond strength of deformed steel fibers increased as fiber spacing decreased due to an additional pressure from adjacent fibers during pullout; (2) straight steel fibers were not influenced by fiber spacing; (3) multiple-fiber specimens exhibited lower bond strength than single-fiber specimens; and (4) the lowest bond strength and energy absorption capacity were observed in the bundled fiber case.

As was reported by Tai's study [15], the loading rate sensitivity of steel fiber varies with fiber type, making it difficult to predict the dynamic pullout behavior based on static pullout test results from previous studies. In addition, to the best of the authors' knowledge, there have been no published studies yet of the fiber spacing effect on the impact pullout behavior of steel fibers in UHPC. Studies on the combined effects of fiber geometry and spacing are required to certainly understand the impact or blast resistance of UHPC reinforced with various types and amounts of steel fibers. Accordingly, the aim of this study is to examine the effects of fiber geometry and spacing on the pullout behavior of steel fibers in UHPC under the static and impact loads. For this, three types of steel fibers (straight, hooked, and twisted), four different fiber spacings (corresponding to either 1%, 2%, and 7% fiber volume fractions or fiber bundles), and three loading rates (static loading and dynamic loading with air pressures of 4 and 8 kN) were considered.

1.1 Research significance

Pullout behavior of steel fibers provides useful information for understanding post-cracking tensile behavior of UHPFRC in detail. Although pullout behavior of single steel fiber embedded in UHPC has been investigated in the past, research on the fiber pullout behavior of multiple steel fibers embedded in UHPC is very limited [12, 19]. Moreover, recently published studies have shown that UHPFRC

Table 1 Mixture proportions

W/B[a]	Unit weight (kg/m^3)					
	Water	Cement	Silica fume	Silica sand	Silica flour	SP[b]
0.2	160.3	788.5	197.1	867.4	236.6	52.6

W/B water-to-binder ratio, *SP* superplasticizer

[a]*W/B* is calculated by dividing total water content (160.3 kg/m^3 + 36.8 kg/m^3) by total amount of binder (788.5 kg/m^3 + 197.1 kg/m^3)

[b]Superplasticizer includes 30% solid (= 15.8 kg/m^3) and 70% water (= 36.8 kg/m^3)

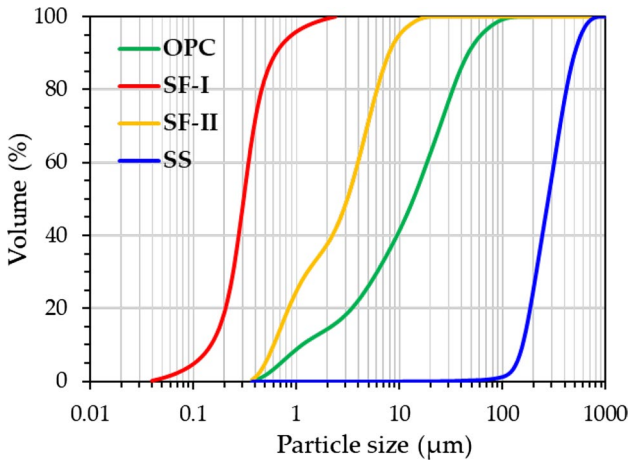

Fig. 1 Particle size distribution of raw materials (ordinary Portland cement (OPC), silica fume (SF-I), silica flour (SF-II), and silica sand (SS)) [20]

exhibits a fairly low correlation between single-fiber pullout behavior and tensile behavior of UHPFRC [17, 18]. Therefore, in an attempt to increase the correlation, it is likely that multiple-fiber pullout tests under various conditions would be beneficial in predicting tensile behavior of UHPFRC. This study investigated the effects of fiber spacing on the pullout behavior of various steel fibers embedded in UHPC under static and impact loads.

2 Experimental program

2.1 Raw materials and mixture proportions

To fabricate UHPC, two cementitious materials, Type I Portland cement and silica fume (SF), were used, and their specifications are given in Table 1. Silica sand with grain size ranging from 0.2 to 0.3 mm and silica flour with a diameter of about 4.2 μm were adopted as a fine aggregate and filler, respectively. The detailed particle size distribution of raw materials for the silica fumes and other fines used in this study is shown in Fig. 1 [20]. Since addition of coarse aggregate deteriorates fiber pullout resistance and post-cracking tensile performance, it was not included in the mixture of UHPC as in previous studies [1, 21]. UHPC mixture with the range of compressive strength over 180 MPa which is optimized for steel fibers was referred from the study by Park et al. [22], and it had a very low water-to-binder (*W/B*) ratio of 0.2. To counteract this, a high-range water-reducing admixture, called a superplasticizer (SP), was added into the mixture to improve the workability and to achieve a self-consolidating property. The detailed mix proportions of the UHPC used in this experiment are summarized in Table 2. The identical mix proportion was applied for all of the tested samples.

Table 2 Chemical compositions and physical properties of cement and silica fume

Composition (%) (mass)	Type I Portland cement	Silica fume
CaO	61.33	0.38
Al_2O_3	6.40	0.25
SiO_2	21.01	96.00
Fe_2O_3	3.12	0.12
MgO	3.02	0.10
SO_3	2.30	–
Specific surface area (cm^2/g)	3413	200,000
Density (g/cm^3)	3.15	2.10

The aim of this study is to examine the effects of fiber geometry and fiber volume fraction (or spacing) on the pullout behaviors of steel fibers embedded in UHPC at various loading rates ranging from 0.018 mm/s (static) to 740 mm/s (impact). Dog-bone-shaped specimens were fabricated for evaluating the pullout behaviors, and three different types of steel fibers, e.g., straight, hooked, and twisted, were embedded in the UHPC and pulled out under the static and impact loads. Three different fiber spacings, corresponding to fiber volume fractions of 1, 2, and 7%, were studied. To analyze the group effect of fibers, bundle-type specimens with zero fiber distance were also fabricated, along with single-fiber specimens as control specimens. The geometrical details of the straight, hooked, and twisted fibers are as follows: The aspect ratio (l_f/d_f) of the straight and hooked fibers was 30/0.3 mm/mm = 100, and that of the hooked fibers was 30/0.375 mm/mm = 80, where l_f is the fiber length and d_f

is the fiber diameter. The geometric and physical properties of the steel fibers are shown in Fig. 2 and given in Table 3.

2.2 Mixing sequence and curing regime

Since UHPC mixtures have low W/B ratios and low self-consolidating properties, a special mixing sequence was adopted for the concrete in this study. The dry ingredients, such as cement, SF, silica sand, and silica flour, were premixed for about 10 min for effective dispersion. Water, premixed with SP, was then added to the dry ingredients, and an additional 10 min of mixing was performed until the mixture became flowable. After that, the fibers were fixed in the desired positions (center) in the dog-bone-shaped molds, and the fresh UHPC mixture was cast into only one side of the mold and cured for 2 days at room temperature. After removing the fiber fixture, fresh UHPC was cast into the other side of the mold and cured for another 2 days at the same room temperature. Then, the specimens were demolded and steam cured at 90 ± 2 °C for 3 days to accelerate strength development. The specimens were then taken out of the water tank and dried at room temperature before the pullout tests.

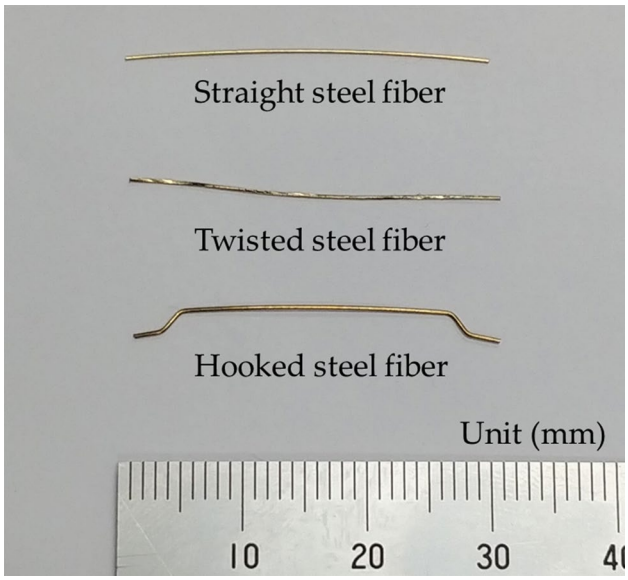

Fig. 2 Geometric properties of steel fibers

2.3 Specimen preparation

For this study, the fibers were vertically embedded in a 2×2 array at the center of dog-bone-shaped specimens. The cross-sectional area of each dog-bone-shaped specimen was 25×25 mm^2, as shown in Fig. 3. We assumed that the fibers were aligned in the direction of tensile load and uniformly distributed in two dimensions. If so, the fiber volume fraction becomes equal to the cross-sectional area ratios occupied by the fibers and the composites, then the fiber distances were determined. The distances between the straight and twisted fibers were calculated to be about 2.7, 1.9, and 1.0 mm for volume fractions of 1%, 2%, and 7%, respectively, at which the distances between the hooked fibers were calculated to be about 3.3, 2.4, and 1.2 mm, as summarized in Table 4. The differences in fiber spacing, which is a center-to-center distance, were caused by the different fiber diameters (0.3 and 0.375 mm). Since it is almost impossible to perfectly, uniformly disperse the fibers in the UHPC matrix, fiber bundles are easily observed in the UHPFRC composites. To evaluate the effect of fiber bundles on the pullout behaviors, additional specimens with multiple fibers with a zero spacing were fabricated. All fibers had a length of 30 mm. Different embedment lengths were applied on the two sides of the dog-bone-shaped specimens to allow the fibers to be pulled out from only one side with a shorter embedment length. Shorter embedment lengths of 10 mm were used for the straight and hooked steel fiber cases, while to prevent fiber rupture, a shorter embedment length of 5 mm was adopted for the twisted steel fiber specimens. The notation of the fiber specimen is composed of the fiber type, volume ratio, and loading condition. The capital letters S, H, and T indicate straight, hooked, and twisted steel fibers, respectively, and the subsequent numeral (1, 2, and 7) or capital letters (B and S) indicate the volume fractions of 1, 2, and 7% or fiber bundle and single fiber. The last letter denotes static load or 4- and 8-kN impact loads. For example, S-1–4 kN indicates straight steel fiber with a volume fraction of 1% under the 4-kN impact load.

Table 3 Geometrical and physical properties of steel fibers

	d_f (mm)	l_f (mm)	Aspect ratio (l_f/d_f)	Density (g/cm^3)	f_{ft} (MPa)	E_f (GPa)
S	0.300	30.0	100.0	7.9	2580	200
H	0.375	30.0	80.0	7.9	2900	200
T	0.300	30.0	100.0	7.9	2428	200

S, straight steel fiber; H, hooked steel fiber; T, twisted steel fiber; d_f, fiber diameter; l_f, fiber length; f_{ft}, tensile strength of fiber; and E_f, elastic modulus of fiber

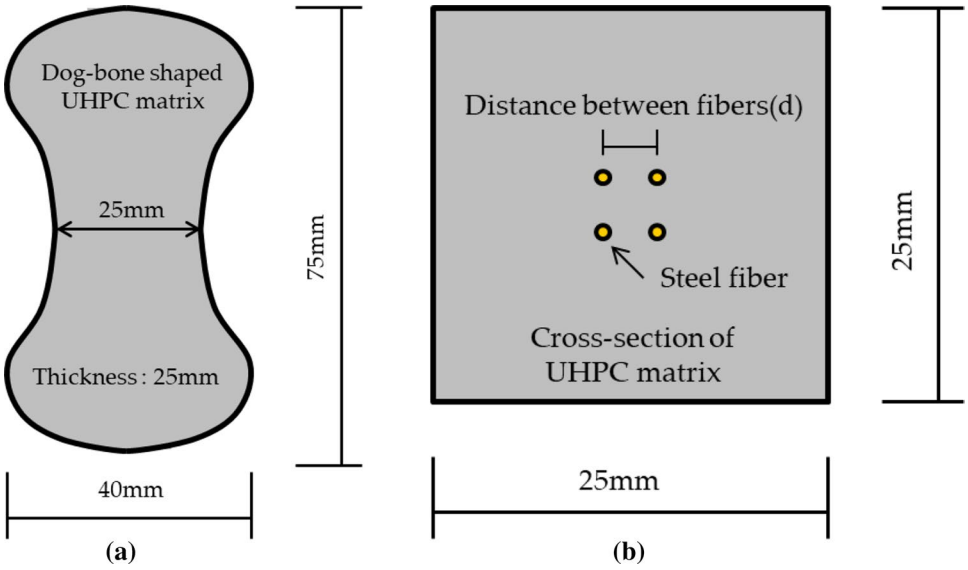

Fig. 3 Schematic description of dog-bone-shaped specimen: **a** dimensions, **b** details of fiber location

2.4 Experimental setup and procedure

A universal testing machine (UTM) was used for evaluating static pullout performance. The applied load was measured using a load cell affixed to the machine with a maximum capacity of 3 kN. The dog-bone-shaped specimen was inserted into the steel jig grip system, and the pullout load was monotonically applied at a rate of 0.018 mm/s. Based on an assumption that the elastic deformations of the specimen and steel jig are negligible, the fiber's end slip was directly measured as stroke displacement. The detailed test setup for the static pullout tests is shown in Fig. 4a.

It is well known that UHPFRC is superior to ordinary concrete under extreme loading conditions (e.g., impact and blast) [23, 24]. Aoude et al. [23] noted that UHPFRC significantly improves the blast resistance of columns compared to ordinary self-consolidating concrete in terms of lower maximum and residual displacements at equivalent blast loads and an ability to sustain larger blast loads before failure. Krauthammer [24] has reported that, although a UHPFRC column becomes more susceptible to transverse loads at high axial load levels than a normal-strength concrete column, it can sustain more than four times the load before failure. To understand the behavior of UHPFRC under extreme loads, the fiber pullout behavior must be examined at higher loading rates. A pullout impact test machine was specially fabricated for this study. The dog-bone-shaped specimen was first inserted into the steel jig grip and tightly fixed to the machine. The loading rate was determined by controlling the magnitude of the air pressure, and two different air pressure levels (4 and 8 kN) were applied to the specimen through a piston. Yoo and Kim [25] reported that the higher air pressure can give faster loading rate: The air pressures of 2 and 8 kN lead to loading rates of about 480 and 4800 mm/s, respectively, without the specimen. To exclude the specimen's inertia, a load cell with a maximum capacity of 10 kN was affixed to the test machine on the opposite side to the loading piston. A potentiometer with a capacity of 10 cm was fixed to the steel frame of the piston and used to measure the vertical movement of the loading piston. A hinge-type grip system, which allows a slight rotation of the specimen, was also adopted at the opposite side to the loading piston to minimize the eccentric effect. By assuming that the elastic deformations of the specimen, steel jig, and frame were negligible, the displacement measured from the potentiometer was used as the fiber slip value. In order to obtain sufficient data points, data were collected using a dynamic data acquisition system with a frequency of 20 kHz. The detailed test setup for the impact fiber pullout tests is shown in Fig. 4b.

3 Experimental results and discussion

3.1 Pullout load–slip response

The average pullout load versus slip ($P-S$) curves for each of the steel fiber types embedded in the UHPC under various loading rates are shown in Figs. 5, 6, and 7. To obtain reliable test results, five specimens were fabricated and tested for each variable, and an average of the resulting five $P-S$ curves was adopted. With regard to the pullout behavior of straight steel fibers in UHPC (Fig. 5), the multiple-fiber specimens generally showed similar-shaped curves regardless of fiber spacing, and no significant change occurred with changes in loading rate. When fibers are bundled, the bonding area of each fiber adhering to the matrix decreases. Thus, the bundled fiber specimens under the static rate showed the smallest maximum pullout load compared to the other

Table 4 Test variables

Specimens	Fiber type	Corresponding fiber volume fraction (%)	Distance between fibers[a] (mm)
S-1-static/4 kN/8 kN	Straight	1.0	2.7
S-2-static/4 kN/8 kN		2.0	1.9
S-7-static/4 kN/8 kN		7.0	1.0
S-B-static/4 kN/8 kN		–	0.0
S-S-static/4 kN/8 kN		–	–
H-1-static/4 kN/8 kN	Hooked	1.0	3.3
H-2-static/4 kN/8 kN		2.0	2.4
H-7-static/4 kN/8 kN		7.0	1.2
H-B-static/4 kN/8 kN		–	0.0
H-S-static/4 kN/8 kN		–	–
T-1-static/4 kN/8 kN	Twisted	1.0	2.7
T-2-static/4 kN/8 kN		2.0	1.9
T-7-static/4 kN/8 kN		7.0	1.0
T-B-static/4 kN/8 kN		–	0.0
T-S-static/4 kN/8 kN		–	–

1, 2, and 7 = fiber spacing corresponding to the volume fractions of 1, 2, and 7%, B = fiber bundle, S = single fiber, and static/4 kN/8 kN = type of applied loads

[a]Distance between fibers is corresponding to the fiber volume fraction

multiple-fiber specimens [19]. However, under the impact loads, the bundled fiber specimens provided the higher pullout resistance than those of the other multiple-fiber specimens. The pullout resistance of bundled fibers was very high at the beginning of the fiber slip, whereas their decrease rate on the pullout resistance was steeper. After a slip of about half the fiber embedment length, the bundled fiber specimen's pullout resistance was rather smaller than those of other multiple-fiber specimens at the impact condition.

The $P-S$ curves of hooked steel fibers in UHPC under various loading rates are shown in Fig. 6. The post-peak pullout resistance of hooked fiber was reduced rapidly since the maximum pullout resistance depends on the mechanical anchorage effect of the end hooks. Except for cases of fiber rupture or severe matrix failure, the multiple hooked fibers in UHPC showed similar $P-S$ curve shapes regardless of fiber spacing and loading rate. According to a previous study [19], hooked fibers affect the pullout resistance of adjacent fibers because they exert pressure on the adjacent fibers. Under the static condition, the maximum pullout load of multiple hooked fibers improved as fiber spacing decreased due to additional pressure from the adjacent fibers through the matrix. However, the multiple hooked fibers showed an opposite tendency for pullout behaviors under the impact loads. For the multiple hooked fibers at the impact loading conditions, fiber rupture occurred in the 1% fiber volume specimens, which is the largest fiber spacing, since they could not withstand the maximum fiber tensile stress with the increased bond strength according to loading rate. As fiber spacing decreased, the amount of the matrix between fibers decreased. If there was not a sufficient volume of matrix around the fibers, the UHPC is not able to withstand the pullout resistance owing to premature failure of matrix. Hooked fiber also increases the damage to the matrix as loading rate increases. Therefore, the matrix failed prematurely, and the hooked fiber pulled out without fracture at smaller spacings.

Figure 7 exhibits the average $P-S$ curves for single, multiple, and bundled twisted steel fibers in UHPC under static and impact loads. The triangular cross-sectional shape of twisted fiber and its twisting along the length act as a mechanical bond. In contrast to the hooked fiber, the twisted fiber has a uniform shape and mechanical bond along the length. Thus, its pullout resistance was proportional to the embedment length. After peak load, the pullout resistance of twisted fibers decreased in a relatively constant manner. Compared to other multiple-fiber cases, the bundled twisted fibers exhibited poorer pullout resistance under the static condition. However, under impact conditions, they showed higher maximum pullout loads than the other multiple-fiber cases, along with severe matrix spalling.

Figures 6 and 7 illustrate that, for the $P-S$ curves of hooked and twisted fibers, there are some cases in which the ultimate slip, zeroing the pullout load, was shorter than the initially embedded length of the fiber. This indicates that the fiber was not fully pulled out either because fiber fracture occurred or because the matrix was severely damaged. Figure 8a is a picture of the hooked fiber and matrix, while Fig. 8b is a picture of bundled twisted fibers after fiber pullout from the matrix. The hooked fibers with a spacing corresponding to the 1% fiber volume showed a fiber rupture, while the bundled hooked fibers caused severe matrix spalling without rupture. The end hooks of bundled hooked fibers were not straightened even after the complete pullout from the matrix, indicating that the severe matrix spalling was generated slightly before reaching the peak pullout load. In addition, the pullout loads of bundled twisted fibers in UHPC under the impact loads dropped to almost zero before reaching the initial embedment length of 5 mm (Fig. 7). As

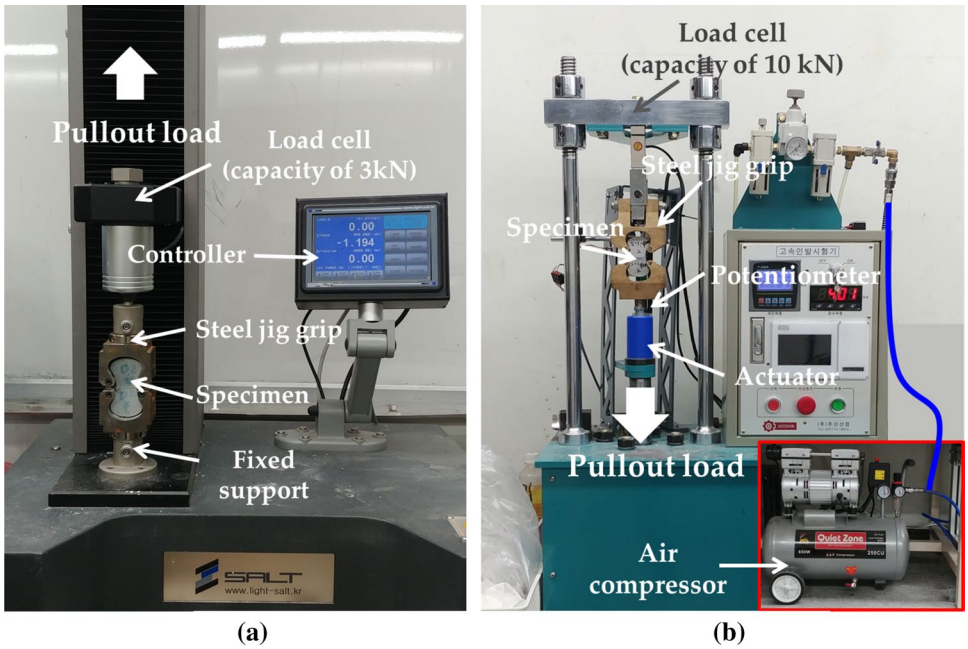

Fig. 4 Fiber pullout test setups with different loading rates of **a** quasi-static and **b** impact

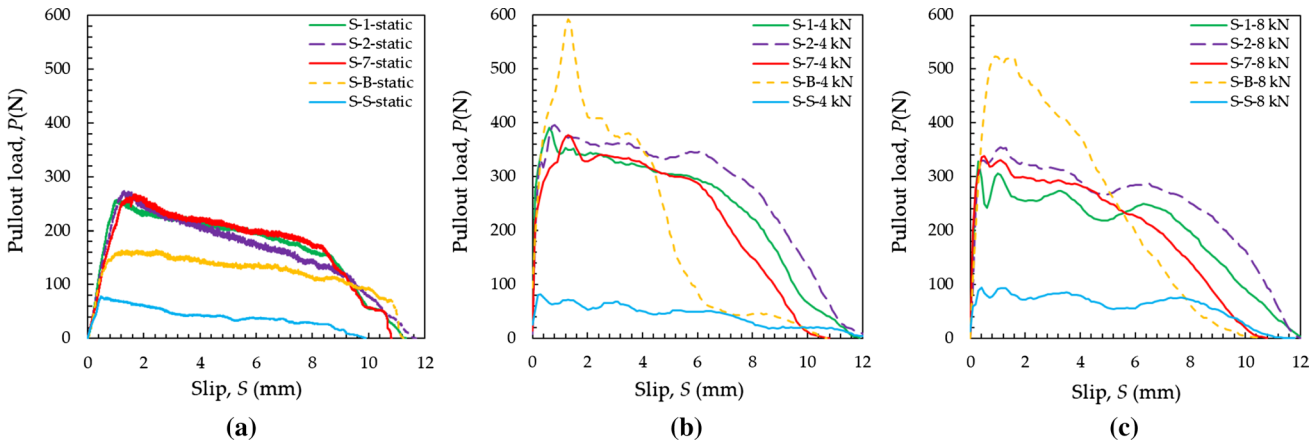

Fig. 5 Straight steel fiber pullout load versus slip responses curves: **a** quasi-static, **b** 4-kN impact, and **c** 8-kN impact

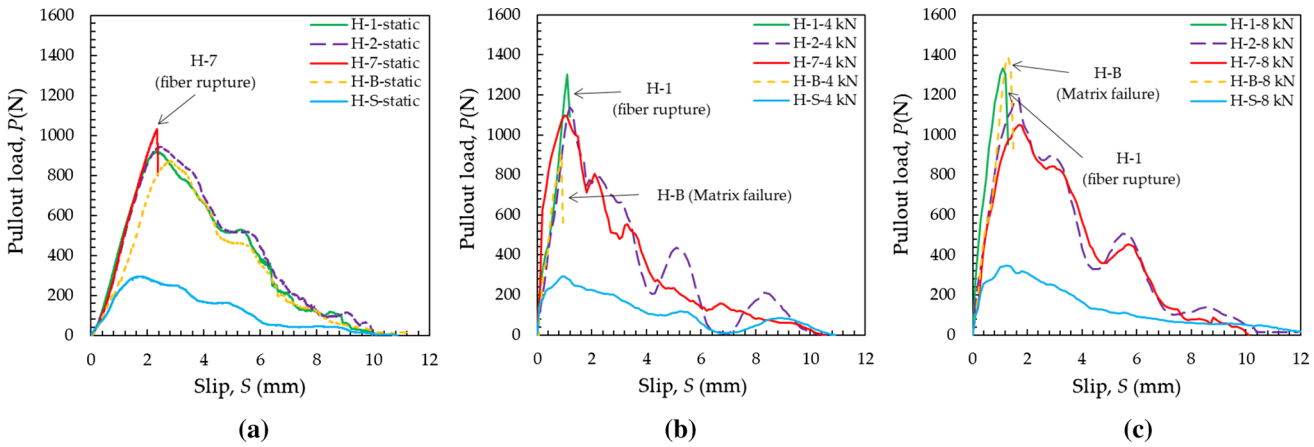

Fig. 6 Hooked steel fiber pullout load versus slip responses curves: **a** quasi-static, **b** 4-kN impact, and **c** 8-kN impact

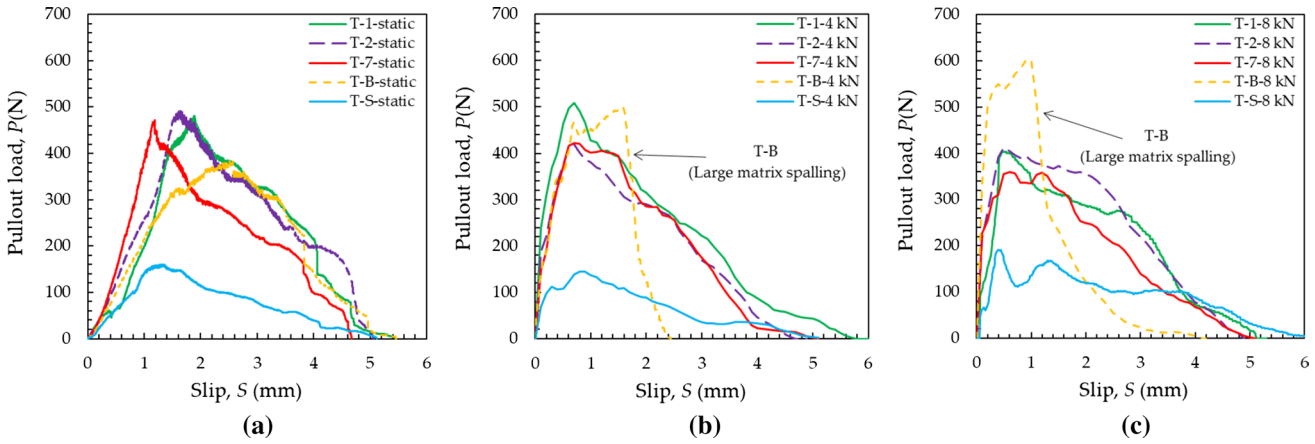

Fig. 7 Twisted steel fiber pullout load versus slip responses curves: **a** quasi-static, **b** 4-kN impact, and **c** 8-kN impact

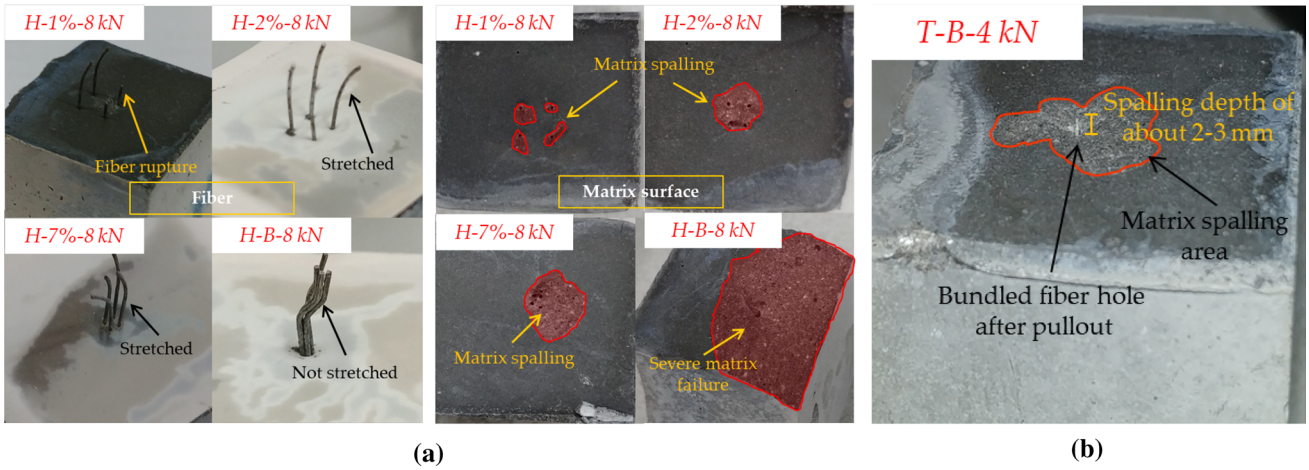

Fig. 8 Comparative pullout failure modes of deformed steel fiber: **a** hooked fibers and **b** twisted fibers

shown in Fig. 8a, b, portion of the matrix with embedded fibers was severely damaged under the impact loads, and the depth of matrix damage was about 1−3 mm, reducing the ultimate slip of about 2 to 3 mm in Fig. 7b, c.

3.2 Effects of fiber geometry and spacing on pullout parameters

3.2.1 Average bond strength

Important pullout parameters according to fiber geometry, spacing, and loading rates are summarized in Tables 5 and 6, and the average bond strength (τ_{av}), which is one of the important pullout parameters, is given in Fig. 9. The average bond strength was calculated in terms of the maximum pullout load and bonding area between the fiber and matrix, as follows:

$$\tau_{av} = \frac{P_{max}}{\pi d_f L_E} \quad (1)$$

where τ_{av} is the average bond strength, P_{max} is the maximum pullout load, d_f is the fiber diameter, and L_E is the actual initial embedded length of the fiber.

The average bond strength of the single straight steel fiber in UHPC was 8.8 MPa under static loading. Under the impact loading conditions with the loading rates of 441.1 mm/s and 740.3 mm/s, the average bond strength increased by about 38% and 68%, respectively. The bundled fibers showed the largest increase in average bond strength, followed by single fiber and then multiple fibers, corresponding to the volume fractions of 7%, 2%, and 1%. Multiple straight steel fibers with smaller spacings were more sensitive to the loading rate than those with larger spacings. Specifically, the bundled fibers showed an increase in average bond strength of about 220−308% under impact loads.

Table 5 Summary of DIF of maximum pullout load depending on fiber types, spacing, and loading rate

Fiber type	Corresponding fiber volume fraction	Quasi-static			4-kN air pressure			8-kN air pressure		
		P_{max} (N)	DIF	Rate (mm/s)	P_{max} (N)	DIF	Rate (mm/s)	P_{max} (N)	DIF	Rate (mm/s)
Straight	1%	277.1	1.00	0.018	400.8	1.44	504.5	355.6	1.21	629.9
	2%	279.4	1.00	0.018	432.0	1.55	610.2	405.6	1.45	667.3
	7%	280.0	1.00	0.018	401.7	1.43	558.5	371.0	1.32	593.8
	Bundle	170.5	1.00	0.018	567.9	3.33	525.5	644.7	3.78	589.1
	Single	82.0	1.00	0.018	120.6	1.47	441.1	149.7	1.83	740.3
Hooked	1%	937.9	1.00	0.018	1351.9	1.28	380.5	1377.4	1.47	420.4
	2%	956.6	1.00	0.018	1157.9	1.37	373.3	1262.8	1.32	588.2
	7%	1081.3	1.00	0.018	1177.9	1.32	317.4	1140.1	1.05	597.3
	Bundle	884.1	1.00	0.018	1383.9	1.57	328.0	1300.0	1.47	421.8
	Single	320.3	1.00	0.018	339.9	1.74	376.3	363.7	1.13	617.7
Twisted	1%	494.4	1.00	0.018	555.1	1.12	335.1	420.2	0.85	498.2
	2%	494.0	1.00	0.018	460.2	0.93	279.7	472.1	0.96	483.0
	7%	476.1	1.00	0.018	488.2	1.03	317.3	383.7	0.81	676.9
	Bundle	454.6	1.00	0.018	551.3	1.21	389.3	642.6	1.41	423.3
	Single	165.8	1.00	0.018	165.9	1.00	400.8	193.9	1.17	515.2

This is significantly higher than the increases of other multiple-fiber specimens, showing about 21−55% increases, and the single-fiber specimen. Pacios et al. [26] reported that increasing the number of fibers from 8 to 16 with a decrease in the fiber spacing was effective in increasing the loading rate sensitivity but ineffective in changing the average bond strength, consistent with the findings of this study for the case of straight steel fiber.

The rate sensitivity on the average bond strength was higher for the multiple fibers with closer spacings, as shown in Fig. 9. The multiple fibers with closer spacings were more effective in enhancing the pullout resistance than those with wider spacings, because of the mitigation of eccentric effect according to the previous study by Yoo et al. [27]. They [27] also reported the gap between the fibers was filled with fresh UHPC due to their curly-shaped configuration, and this resulted in a larger diameter of the fiber bundle at the end. Since the impact load was applied instantly and the bundle of fibers had a larger diameter at the end, mechanical anchorage was additionally generated, resulting in the highest average bond strengths at the impact loads.

The single hooked fiber embedded in UHPC exhibited an average bond strength of about 27.2 MPa under the static load, with increases of 6% and 14% for impact loads with rates of 376.3 and 617.7 mm/s, respectively. This means that the rate sensitivity to average bond strength was higher for the straight steel fiber in UHPC, compared to that of the hooked steel fiber. The static average bond strengths increased by 3% and 17% when fiber spacings were reduced from 3.3 mm (1% fiber volume fraction) to 2.4 mm and 1.2 mm (2% and 7% fiber volume fraction), respectively. The average static bond strength of multiple fibers with a spacing of 3.3 mm was found to be 19.7 MPa. However, the bundled hooked fiber specimens exhibited the lowest average bond strength of 18.8 MPa. Under the impact loading conditions, the average bond strength decreased with decreasing fiber spacing, and the bundled fiber specimens showed the higher average bond strength than the other multiple-fiber specimens, with an exception of the 1% fiber volume specimen. The average bond strength is directly related to the maximum pullout load. In addition, the trend of decreasing average bond strength as the fiber spacing decreases can be explained by the premature matrix damage that occurred due to the loading rate effect and decreased fiber spacing. The reduced matrix volume with a result of the decreased fiber spacing adversely affected the matrix from being able to endure the increased fiber pullout load.

The single twisted fiber specimens showed a marked increase in average bond strength as the loading rate increased. The static average bond strength was about 38.3 MPa, increasing 15% and 19% at the impact loading conditions with rates of 400.8 and 515.2 mm/s, respectively. This indicates that the rate sensitivity of twisted fiber in UHPC to average bond strength is between those of the straight and hooked fiber cases. Unlike the other fiber types, multiple twisted fibers exhibited no significant tendency to increase or decrease with loading rate, but single and bundled twisted fibers tended to increase. Even the multiple twisted fibers with closest spacing (1.0 mm) showed smaller average bond strengths under impact loads than when under the static loading. Under the static condition, the average bond strength of the specimens with multiple twisted fibers increased with increasing fiber spacing owing to the pressure applied to the adjacent fibers during pullout. For example,

Table 6 Summary of pullout parameters depending on fiber type, spacing, and loading rate

Fiber type	Corresponding fiber volume fraction	Parameters	Quasi-static	4-kN air pressure	8-kN air pressure
Straight	1%	W_p ($\times 10^{-3}$ J)	1935.3 (39.03)	2888.2 (178.19)	2414.5 (371.43)
		$\sigma_{f,max}$ (MPa)	979.9 (137.88)	1417.7 (55.56)	1186.7 (632.64)
		τ_{av} (MPa)	6.19 (0.53)	8.42 (0.71)	7.47 (0.41)
		τ_{eq} (MPa)	8.99 (1.55)	9.57 (0.76)	9.08 (2.07)
	2%	W_p ($\times 10^{-3}$ J)	1693.2 (50.01)	3294.6 (943.67)	2939.9 (341.21)
		$\sigma_{f,max}$ (MPa)	988.03 (18.03)	1527.8 (272.92)	1434.7 (297.81)
		τ_{av} (MPa)	6.91 (0.78)	9.04 (1.98)	9.10 (1.98)
		τ_{eq} (MPa)	8.35 (1.46)	10.97 (4.18)	11.18 (1.57)
	7%	W_p ($\times 10^{-3}$ J)	1886.10 (631.65)	2581.7 (358.51)	2246.3 (969.95)
		$\sigma_{f,max}$ (MPa)	990.38 (227.82)	1420.7 (131.89)	1312.0 (517.75)
		τ_{av} (MPa)	6.81 (2.40)	9.37 (1.28)	9.94 (3.76)
		τ_{eq} (MPa)	8.81 (3.24)	10.58 (2.00)	12.01 (4.29)
	Bundle	W_p ($\times 10^{-3}$ J)	1300.3 (170.05)	2460.8 (131.63)	2881.1 (918.57)
		$\sigma_{f,max}$ (MPa)	603.05 (61.33)	2008.5 (236.56)	2280.3 (723.81)
		τ_{av} (MPa)	4.26 (0.91)	13.63 (1.43)	17.36 (5.92)
		τ_{eq} (MPa)	6.70 (2.08)	10.53 (1.31)	15.74 (5.26)
	Single	W_p ($\times 10^{-3}$ J)	400.9 (131.61)	681.4 (173.37)	837.4 (248.77)
		$\sigma_{f,max}$ (MPa)	1159.8 (189.92)	1705.9 (236.56)	2117.7 (621.59)
		τ_{av} (MPa)	8.82 (1.65)	12.13 (1.43)	14.80 (3.39)
		τ_{eq} (MPa)	8.82 (2.91)	12.85 (1.31)	14.51 (5.57)
Hooked	1%	W_p ($\times 10^{-3}$ J)	4640.3 (1212.71)	1063.1 (262.77)[b]	1339.8 (109.99)[b]
		$\sigma_{f,max}$ (MPa)	2098.4 (291.39)	3060.2 (318.16)[b]	3117.8 (64.07)[b]
		τ_{av} (MPa)	19.67 (2.73)	28.69 (2.98)[b]	29.23 (0.60)[b]
		τ_{eq} (MPa)	19.69 (5.15)	4.51 (1.12)[b]	5.69 (0.47)[b]
	2%	W_p ($\times 10^{-3}$ J)	4752.2 (471.53)	3730.0 (234.03)	4498.2 (667.07)
		$\sigma_{f,max}$ (MPa)	2165.3 (86.68)	2620.9 (185.61)	2858.4 (21.84)
		τ_{av} (MPa)	20.30 (2.62)	24.57 (1.74)	26.80 (0.21)
		τ_{eq} (MPa)	20.17 (3.91)	15.83 (0.99)	19.09 (2.83)
	7%	W_p ($\times 10^{-3}$ J)	3940.5 (921.45)[b]	3235.4 (878.80)	4188.8 (327.07)
		$\sigma_{f,max}$ (MPa)	2447.5 (279.12)[b]	2666.2 (39.88)	2580.7 (16.76)
		τ_{av} (MPa)	22.95 (2.62)[b]	25.00 (0.37)	24.19 (0.16)
		τ_{eq} (MPa)	16.72 (3.91)[b]	13.73 (3.71)	17.78 (1.39)
	Bundle	W_p ($\times 10^{-3}$ J)	3974.1 (733.01)	1097.5 (404.11)[c]	1352.6 (561.91)[c]
		$\sigma_{f,max}$ (MPa)	2001.3 (426.66)	3132.6 (221.76)[c]	2942.7 (454.48)[c]
		τ_{av} (MPa)	18.76 (4.00)	29.37 (2.08)[c]	27.59 (4.26)[c]
		τ_{eq} (MPa)	16.87 (3.11)	4.66 (1.72)[c]	5.74 (2.39)[c]
	Single	W_p ($\times 10^{-3}$ J)	1480.5 (270.42)	1300.6 (175.18)	1749.0 (401.90)
		$\sigma_{f,max}$ (MPa)	2899.7 (482.46)	3077.9 (160.84)	3292.9 (245.60)
		τ_{av} (MPa)	27.18 (4.52)	28.86 (1.51)	30.87 (2.30)
		τ_{eq} (MPa)	25.13 (4.59)	22.08 (2.97)	29.69 (6.82)

Table 6 (continued)

Fiber type	Corresponding fiber volume fraction	Parameters	Quasi-static	4-kN air pressure	8-kN air pressure
Twisted[a]	1%	W_p ($\times 10^{-3}$ J)	1259.5 (94.95)	1310.3 (290.85)	938.8 (275.07)
		$\sigma_{f,max}$ (MPa)	1748.7 (74.28)	1963.4 (206.74)	1486.0 (208.39)
		τ_{av} (MPa)	26.23 (2.59)	28.25 (3.83)	26.25 (7.92)
		τ_{eq} (MPa)	26.73 (4.80)	25.12 (1.53)	27.81 (12.92)
	2%	W_p ($\times 10^{-3}$ J)	1271.1 (107.58)	1042.8 (399.48)	1205.0 (199.39)
		$\sigma_{f,max}$ (MPa)	1747.2 (99.41)	1627.5 (263.53)	1669.6 (224.84)
		τ_{av} (MPa)	26.21 (3.82)	26.05 (2.59)	26.74 (2.10)
		τ_{eq} (MPa)	26.97 (2.73)	24.86 (6.49)	29.27 (3.84)
	7%	W_p ($\times 10^{-3}$ J)	1039.1 (185.94)	1055.7 (287.09)	1012.5 (465.07)
		$\sigma_{f,max}$ (MPa)	1683.9 (115.54)	1726.6 (468.95)	1357.1 (354.32)
		τ_{av} (MPa)	28.08 (0.28)	27.85 (7.57)	23.77 (4.28)
		τ_{eq} (MPa)	27.09 (0.61)	25.78 (6.30)	28.90 (8.82)
	Bundle	W_p ($\times 10^{-3}$ J)	1103.1 (62.92)	784.3 (30.78)	918.9 (359.97)
		$\sigma_{f,max}$ (MPa)	1607.7 (15.73)	1949.7 (230.20)	2272.8 (231.29)
		τ_{av} (MPa)	24.43 (3.16)	29.25 (3.45)	34.09 (3.47)
		τ_{eq} (MPa)	24.65 (5.24)	16.64 (0.65)	19.50 (7.64)
	Single	W_p ($\times 10^{-3}$ J)	386.6 (58.59)	397.1 (201.01)	537.0 (88.24)
		$\sigma_{f,max}$ (MPa)	2345.6 (110.04)	2346.8 (517.99)	2743.6 (638.17)
		τ_{av} (MPa)	38.32 (4.04)	44.00 (9.71)	45.73 (10.64)
		τ_{eq} (MPa)	38.75 (5.90)	52.67 (26.66)	56.28 (9.25)

W_p, pullout work; P_{max}, maximum pullout load; $\sigma_{f;max}$, maximum fiber tensile stress; τ_{av}, average bond strength; τ_{eq}, equivalent bond strength; and (), standard deviation

[a]T specimens with an embedment length of 5 mm

[b]Specimen with fiber rupture

[c]Specimen with matrix failure

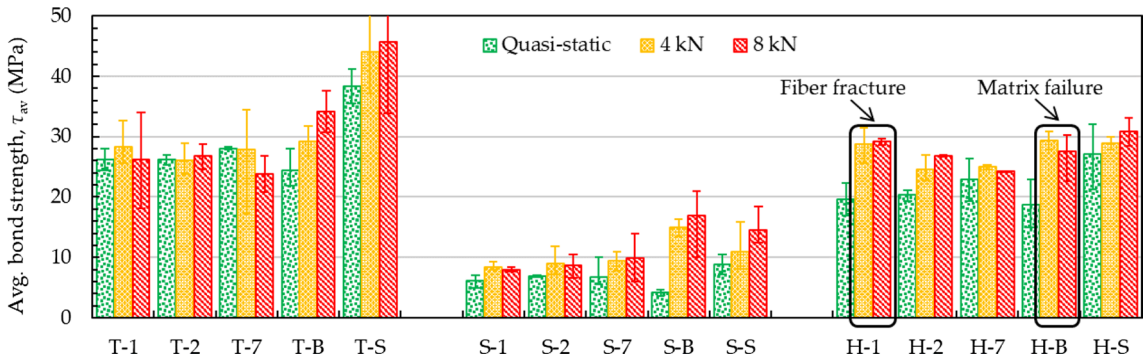

Fig. 9 Summary of average bond strength

the average bond strength increased by about 5% in the closest spacing of 1.0 mm compared to the farthest spacing of 2.7 mm. However, under impact conditions, there was no clear trend in average bond strengths of the multiple twisted fibers according to spacing, with results varying from − 15 to + 8%. Furthermore, since the bundled twisted fiber

specimens provided the highest rate sensitivity, the higher average bond strength under the impact loading conditions was obtained in the bundled fiber specimen compared to the other multiple-fiber specimens. The differences between the average bond strengths of bundled and multiple-fiber specimens became more obvious at higher loading rate.

3.2.2 Pullout energy and equivalent bond strength

The pullout energy and equivalent bond strength of the fibers are summarized in Table 6 and illustrated in Figs. 10 and 11. The pullout energy represents the energy required to completely pull out the fibers from the matrix. Therefore, the pullout energy, W_p, is calculated based on the area under the pullout load–slip curve and is given by

$$W_p = \int_{s=0}^{s=L_E} P(s)\mathrm{d}s \tag{2}$$

where W_p is the fiber pullout energy, s is the fiber slip, and $P(s)$ is the fiber pullout load according to slip.

Based on the pullout energy, the equivalent bond strength can be calculated by assuming that the shear stress is distributed equally over the entire embedment length of fiber, as follows:

$$\tau_{eq} = \frac{2W_p}{\pi d_f L_E^2} \tag{3}$$

where τ_{eq} is the equivalent bond strength.

Pullout energy is an important parameter for evaluating the post-cracking ductility of UHPFRC composites. Even if the maximum pullout resistance is high, the fiber is unlikely to provide good reinforcement for the composites unless appropriate energy absorption capacity is achieved. In addition, the equivalent bond strength is a useful parameter to expect strain-hardening tensile behavior of composites. As shown in Fig. 10, under static conditions, the pullout energy absorption capacity was highest in the hooked fiber specimens, followed by the straight and then twisted fiber specimens. The embedment length of the twisted fiber was only 5 mm, half the length of the other fiber types. Thus, although it provided the lowest pullout energy, the twisted fiber exhibited the highest equivalent bond strength, followed by the hooked and then straight fibers (Fig. 11).

The equivalent bond strength of single straight steel fibers in UHPC was 8.8 MPa under the static load, which increased by 46% and 65% under impact loads with rates of 441.1 and 740.3 mm/s, respectively. Single twisted fiber exhibited 38.7 MPa of static equivalent bond strength,

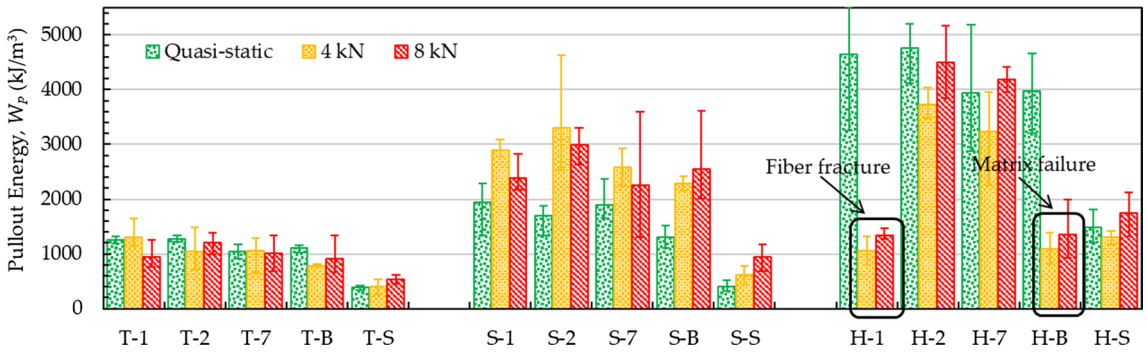

Fig. 10 Summary of fiber pullout energy

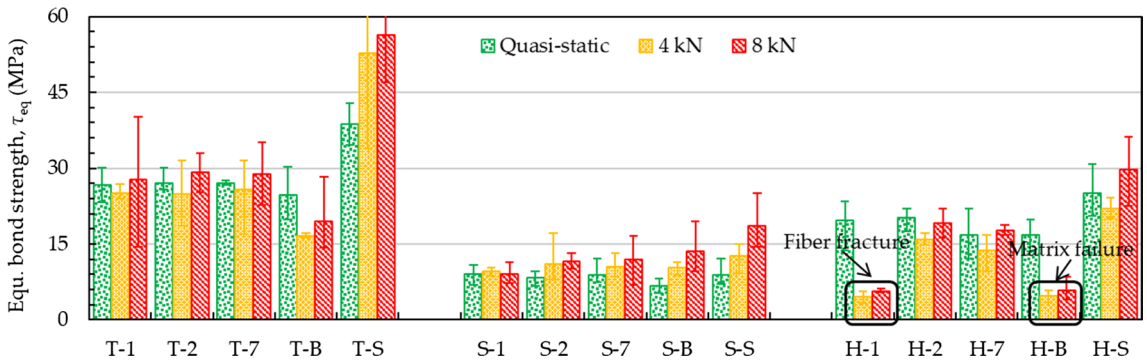

Fig. 11 Summary of equivalent bond strength

which increased by 36% and 45% under the impact loads of 400.8 and 515.2 mm/s, respectively. Contrastingly, the static equivalent bond strength of single hooked fiber decreased by about 12−18% under the impact conditions, from 25.1 MPa at static, because of its rupture failure. Except for the hooked fiber case, the pullout energy and equivalent bond strength of straight and twisted fiber specimens increased with increasing loading rate, and the straight fiber was more rate sensitive than the twisted fiber.

A straight fiber does not affect the surrounding fibers as it is pulled from the matrix. Therefore, the equivalent bond strength of a single straight fiber was quite similar to that of the specimens with the multiple straight fibers. However, when bundled fibers are embedded in the matrix, the adhesion area of fibers with the matrix decreases. Thus, the static pullout energy and equivalent bond strength of the bundled straight fiber specimens were smaller than those of multiple straight fiber specimens. As mentioned above, however, under high loading rates, due to their greater diameter and conical shape at the fiber end, an anchorage effect was activated, causing the energy absorption capacity to be higher than, or at least similar to, those of the other multiple-fiber cases.

The multiple twisted and hooked fiber cases exhibited insignificant changes in equivalent bond strength with loading rate. The twisted and hooked fibers caused matrix damage during pullout [28, 29], thereby deteriorating the adjacent fibers in terms of the pullout energy absorption capacity. Wille et al. [29] explained that the hooked end fiber potentially provides in-plane and/or out-of-plane split cracks due to a highly localized compressive pressure between the fiber and matrix, while the twisted fiber can lead to star-like split cracks since it provides mechanical bond evenly distributed along the embedded length. When fibers were pulled from the matrix with greater resistance and higher maximum pullout load, the matrix damage increased [30], decreasing the total amount of pullout energy absorption capacity of multiple-fiber specimens. For the multiple twisted fiber specimens, except for the bundled twisted fibers, the equivalent bond strength varied with fiber distance and loading rate within about a range of 8%. The bundled twisted fiber specimens showed the lowest equivalent bond strength under both the static and impact loads, and their static equivalent bond strength was reduced by 21−32% under the impact loading conditions. If fiber rupture did not occur, the pullout energies of the multiple hooked fiber specimens were improved when fiber spacing increased. However, there was a clear decrease in pullout energy of multiple hooked fibers with a fiber spacing of 3.3 mm under the impact loads because of their rupture failures. Since the bundled hooked fiber specimens produced severe and premature matrix damage, they also provided poorer pullout energy absorption capacity under the impact loads than those under the static load. The premature matrix failure of bundled hooked fiber specimen is shown in Fig. 8a.

3.2.3 Maximum fiber tensile stress

It is important to design UHPFRC to achieve excellent post-cracking energy absorption capacity, related to fiber's failure mode. A way to simply evaluate the fiber pullout or rupture failure mode is to compare the maximum fiber tensile stress with its ultimate tensile strength. The fiber tensile stress is calculated based on the pullout load and cross-sectional area of the fiber, and the maximum pullout load value can be used for the maximum fiber tensile stress calculation, as follows:

$$\sigma_{\mathrm{f,max}} = \frac{P_{\max}}{A_{\mathrm{f}}} \tag{4}$$

where $\sigma_{\mathrm{f,max}}$ is the maximum tensile stress of fiber and A_{f} is the cross-sectional area of fiber ($=\pi d_{\mathrm{f}}^2/4$).

As summarized in Table 3, each type of steel fiber had a unique tensile strength. If the maximum fiber stress exceeds that tensile strength value, a fiber rupture failure will occur before the fiber is completely pulled out. Since the twisted steel fibers had excellent bond strength at identical embedment lengths of 10 mm, most of them were ruptured before complete pullout. So, a shorter embedded length of 5 mm was applied for the twisted fibers.

The fiber stress of the straight fibers tended to increase consistently with increasing the loading rate. Under impact conditions, the bundled straight fibers exhibited the greatest maximum fiber stress, followed by the single fiber and then other multiple fibers. Straight fiber bundles showed a fiber stress of about 2280 MPa, which is still lower than its tensile strength. Therefore, all variables of straight fibers showed pullout failure mode without a rupture. In the case of twisted fibers, only bundled, and single twisted fibers showed a tendency to increase in maximum fiber stress depending on increasing loading rate; the other multiple fibers (1%, 2%, and 7%) did not show a consistent tendency. At the impact loads, the multiple twisted fibers did not exhibit an obvious trend in maximum fiber stress with variations of fiber spacing and loading rate. Single fiber exhibited the greatest fiber stress, followed by bundled fiber and then other multiple-fiber cases. As mentioned earlier, twisted fiber was embedded only 5 mm in the matrix to prevent fiber fracture, and no fracture occurred in the single fibers, which had the largest maximum fiber stress in all variables. Therefore, the other specimens, all of which had smaller maximum fiber stress, did not exhibit fiber fracture.

Under impact loading conditions, the multiple hooked fibers with a spacing of 3.3 mm showed fiber rupture failure, and the hooked bundled fibers exhibited severe premature matrix damage before their stretchable pullout. This

indicates that they had excellent bond strength and thus had higher maximum fiber stresses than those of the other multiple-fiber cases. However, in Fig. 12, the maximum fiber stress of the hooked fibers of 1% volume was similar to or slightly lower than those of single hooked fiber specimen, which did not exceed the fiber's tensile strength. This phenomenon was considered to be a result of the deviation in maximum pullout load points when the fiber was pulled out. In a previous study [27], even though multiple fibers were pulled from the matrix at the same time, due to their different slip capacities, the maximum pullout load from the average curve was always smaller than the summation of maximum load values from each curve. So, the maximum fiber stress, closely related to the maximum pullout load, of the multiple-fiber specimens was smaller than that of the single-fiber specimens. Furthermore, the magnitude of pullout force for each fiber in a multiple-fiber specimen might be different due to an eccentric effect. Thus, the one with the highest pullout force could rupture prior to pullout of other fibers, leading to the smaller maximum fiber tensile stress.

3.3 Fiber bundling effect

The average and equivalent bond strengths of the bundled fiber specimens under the static conditions were smaller than those of the multiple-fiber specimens due to the decreased bonding area with the matrix regardless of fiber type. However, under the impact loads, all the bundled fiber specimens provided the greatest increases in the average bond strength, higher than most of the other multiple-fiber specimens. The twisted and hooked fibers, however, exhibited much lower pullout energies, despite the increased average bond strengths, since the maximum fiber stresses were closer to or exceeded their tensile strengths, leading to premature rupture failure. Markovic [31] reported that the increase in cross-sectional area of hooked steel fiber leads to increased stiffness and this increases fiber resistance on pullout behavior with enhanced bond strength. The average bond strengths of deformed steel fibers, with their associated larger diameters, would be thus enhanced due to the increase in stiffness since they needed to be stretched to be pulled out from the matrix. The bundling effect in the deformed steel fibers can be explained by the increased stiffness due to the larger total cross-sectional area of the fibers when they are bundled. In order to experimentally verify the stiffness increase, additional experiments were conducted with hooked and twisted steel fibers of the same material with greater diameters (0.9 mm for hooked fiber and 0.5 mm for twisted fiber). Additional pullout tests were conducted under impact load with an air pressure of 8 kN, with the embedment lengths equal to previous tests. As shown in Fig. 13b, the 0.9-mm-diameter hooked fiber's average bond strength and equivalent bond strength were 65% and 38% higher, respectively, than those of the 0.375-mm-diameter hooked fiber. Also, the twisted fiber with 0.5 mm diameter exhibited an increase in average bond strength and equivalent bond strength of 16% and 31%, respectively, compared to the 0.3-mm-diameter twisted fiber. This enhancement in bond strength was due to the increased stiffness and higher cross-sectional area, and it can be inferred that a similar effect was obtained in the bundled hooked and twisted fiber specimens.

Additional pullout tests for the straight fiber were conducted using smaller-sized fibers with a diameter of 0.2 mm. However, the difference between the average bond strengths of the fibers with 0.2 and 0.3 mm diameters was only about 1%. So, we concluded that there was no effect on the average bond strength of straight steel fibers in UHPC with the variations of diameter. However, the bundled straight fiber specimens provided higher average bond strengths under impact loading conditions than the specimens with multiple straight fibers because of the larger diameter of the fiber bundle at the end as explained previously. The larger diameter of the fiber bundles provided additional mechanical anchorage under impact loads, leading to increased pullout resistance.

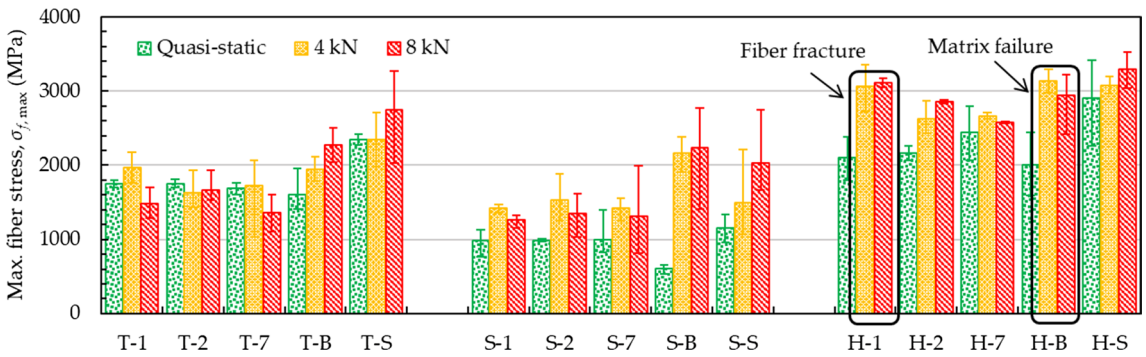

Fig. 12 Summary of maximum fiber tensile stress

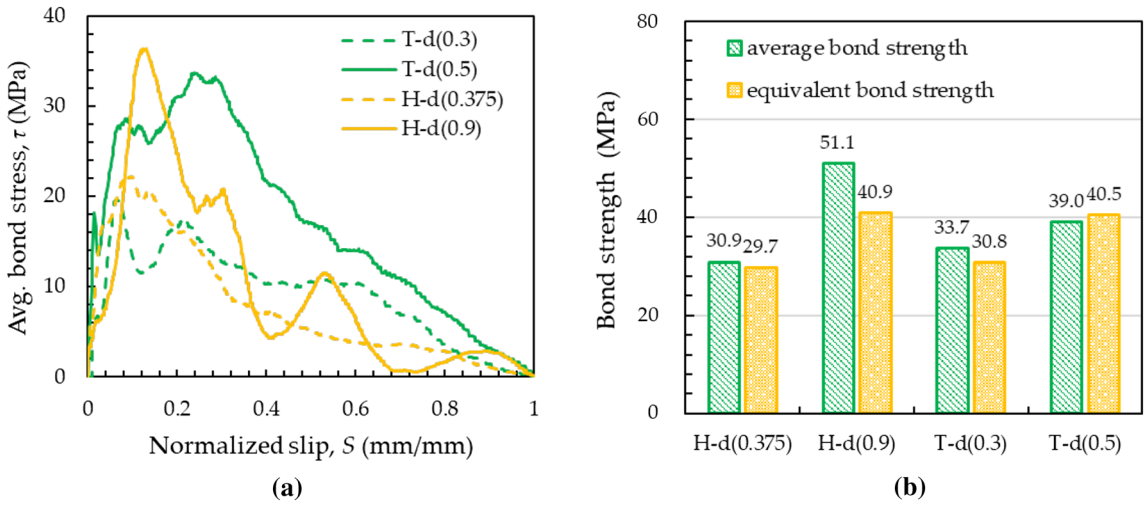

Fig. 13 **a** Average bond stress versus normalized slip curves and **b** bond strength of deformed steel fibers at impact condition (8 kN). *Note* d = diameter (mm)

3.4 Loading rate sensitivity

3.4.1 Determination of loading rate

To analyze the loading rate sensitivity of several pullout parameters, the loading rate was determined based on a speed of fiber slip. The loading rate was not constant with time or magnitude of slip. The loading rate was accelerated with time although the applied air pressure did not vary. The actual displacement (or end slip) of the fibers and the time curves are shown in Fig. 14 with various fiber geometries and air pressures. The displacement and time curves were nonlinear, so that the loading rates were not constant but rather increased with increasing displacement and time. The displacement–time curves varied slightly depending on the fiber geometry (Fig. 14a) but greatly changed according to the magnitude of air pressure (Fig. 14b).

Figure 14a shows that, although the twisted fibers were pulled from the matrix with the same pressure as the other fiber types, they had the fastest loading speed, followed by the straight and then hooked fibers. This means that the loading rate is influenced by the maximum pullout resistance. The average bond strength of deformed fibers is higher than that of straight fibers. However, since the twisted fiber was embedded only 5 mm in the matrix, its reaction force was smallest, and thus, it was accelerated more quickly by the air pressure than those of the straight and hooked fiber specimens. In the same vein, the loading rate increase was

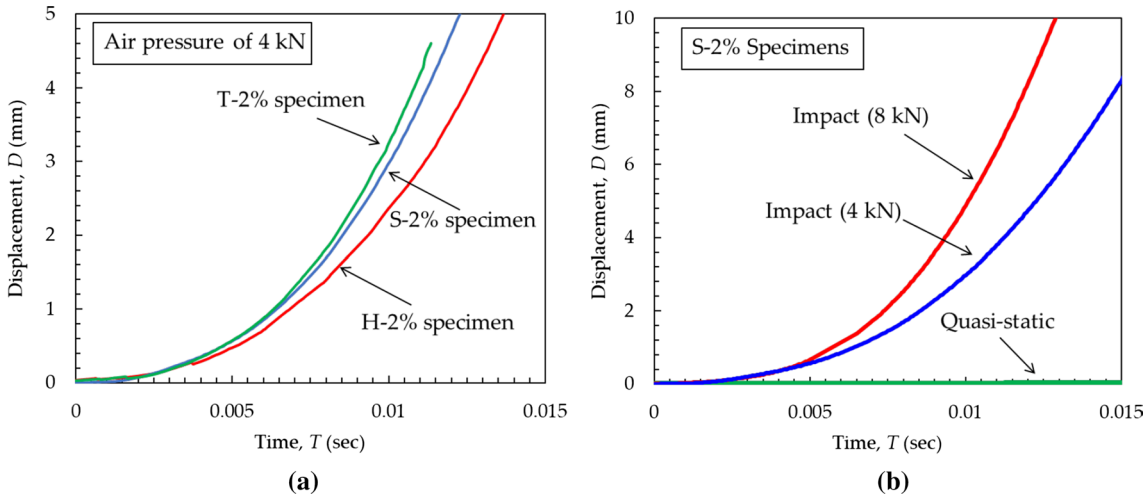

Fig. 14 Displacement–time curves: **a** effect of fiber type and **b** effect of loading condition

higher for the straight fiber specimens than for the hooked fiber case.

The higher air pressure led to the faster loading rate, as shown in Fig. 14b. When the aligned fiber was pulled out, the peak pullout load was attained at the very beginning of slip before the maximum speed was achieved. Thus, to investigate the precise loading rate effect on pullout resistance, it is necessary to measure the exact loading rate at the point of maximum load. Wang et al. [32] reported that strain rate is relatively constant when applied stress exceeds 80% of the ultimate strength under compression and recommended use of the mean value of the strain rate under this condition. Accordingly, for the loading rate in this study, we adopted the average loading rate when the stress exceeded 80% of the ultimate strength. The calculated loading rates are summarized in Table 5.

3.4.2 Effects of fiber geometry and spacing on the rate sensitivity of pullout parameters

Figure 15 shows the dynamic increase factor (DIF) on the average bond strength and loading rate relationships of the straight, hooked, and twisted fibers in UHPC with various fiber spacings. As shown in Fig. 15a, the DIF values of the straight fiber specimens increased steadily in all specimens. The single straight fiber specimens had DIF values ranging from 1.47 to 1.83, while the bundled straight fiber specimens showed the largest increase in DIF, from 3.33 to 3.78. The multiple-fiber specimens showed lower rate sensitivity than the single and bundled cases, and the rate sensitivity of the multiple-fiber specimens increased with decreasing fiber spacing. The straight fiber spacings corresponding to volume fractions of 1%, 2%, and 7% resulted in DIFs of 1.21−1.45, 1.45−1.55, and 1.32−1.43, respectively. The occurrence of higher rate sensitivity in specimens with smaller fiber spacings is also reported in previous studies [26]. In addition, as the fiber spacing of multiple-fiber specimens decreased, the deviation between the maximum pullout loads of the fibers decreased [27].

As shown in Fig. 15b, the single hooked fiber specimens showed a significant increase in DIF with increasing loading rate, and the multiple hooked fiber specimens showed an overall improvement in DIF with increasing loading rate, regardless of fiber spacing. Among the hooked multiple-fiber specimens, the bundled fiber specimen gave the highest DIF increase, and the DIF values increasing with greater fiber spacing. In a previous study [19] at static loads, multiple-fiber specimens were subjected to expansive pressure during pullout. So, the decrease in fiber distance led to an increase in fiber bond strength. However, the tendency at the impact loads was different; the maximum pullout load and average bond strength tended to decrease with decreasing the fiber spacing. The DIFs of the multiple-fiber specimens with the greatest spacing were 1.44−1.47 at the impact loads. On the other hand, smaller DIF values of 1.21−1.32 and 1.05−1.09 were observed for the multiple hooked fiber specimens with spacings of 2.4 and 1.2 mm, respectively. The reason for the smaller DIFs in the specimens with closer spacings was the premature and severe matrix damage, which limited bond strength.

For the twisted fiber specimens (Fig. 15c), when the fitting curve was compared to the DIF versus loading rate response, the DIF value increased significantly only for the bundled and single-fiber specimens. The DIF of the multiple-fiber specimen with the largest spacing (2.7 mm) increased slightly as the loading rate increased. However, DIFs decreased with increasing loading rate in the specimens with fiber spacings of 1.9 and 1.0 mm. Yoo et al. [21] noted that UHPC with twisted steel fibers exhibited lower loading rate sensitivity on the post-cracking flexural strength under drop-weight impact loads compared to straight steel fibers, which is consistent with the results of this study. Since the post-cracking flexural strength in UHPFRC depends mainly on the fiber pullout resistance, it showed a consistent trend with the fiber pullout test results. Yoo et al. [21] explained

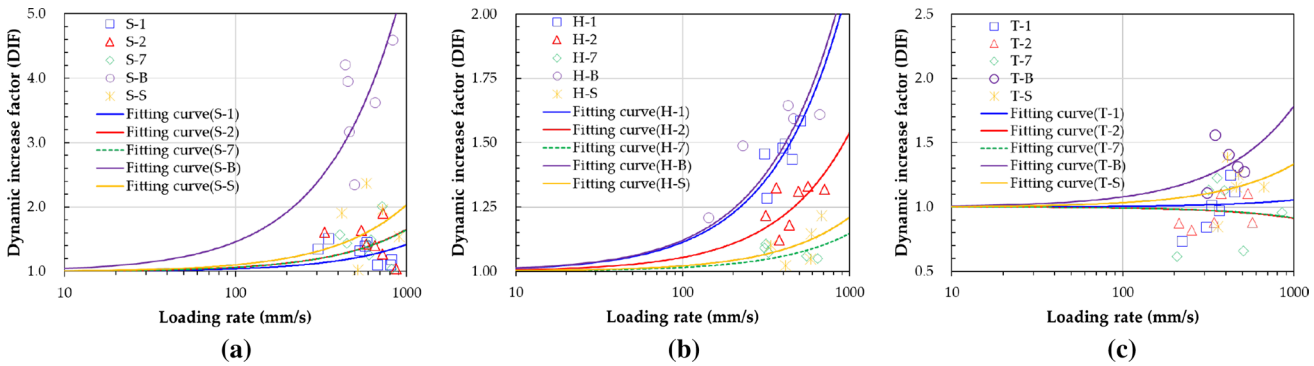

Fig. 15 Summary of dynamic increase factors (DIFs): **a** straight fiber, **b** hooked fiber, and **c** twisted fiber

that the reason for this observation was that the inclined twisted fibers were less rate sensitive. This was verified by Tai and El-Tawil [15]. In their study, the increase in spalling and matrix damage in the fiber pullout test caused the DIF values to drop below 1.00 because of the deteriorated pull-out resistance of inclined twisted fibers in UHPC. However, the aligned single twisted steel fiber specimens tended to have increasing DIFs as the loading rate increased, similar to the observations of this study. The loading rate effect on the pullout behavior of single twisted steel fibers in UHPC was studied by several researchers [15] and reported that the matrix spalling area of twisted fiber specimen increases with loading rate. Moreover, in the case of deformed fibers, Kim and Yoo [19] confirmed that decreasing the fiber spacing led to overlapping of the spalling area of each fiber, and the overlapped matrix spalling area by the adjacent fiber results in a larger spalling area in the matrix. In this study, the spalling generated by each single fiber increased under the impact loading conditions, and matrix spalling became overlapped under the impact loads, which was inconsistent with the static test results, as shown in Fig. 16. Similar to a result in a previous study by Tai and El-Tawil [15], the increased spalling area and matrix damage caused by the adjacent fibers were responsible for the lower rate sensitivity of the twisted fiber specimens compared to other types of fibers, such as straight and hooked fibers.

4 Conclusion

This study investigated the effects of fiber geometry, spacing, and loading rate on the pullout behavior of steel fibers embedded in UHPC. For this, three different types of steel fibers (e.g., straight, hooked, and twisted), four different fiber spacings corresponding to fiber volume fractions of 1, 2, and 7%, plus a fiber bundle, and three different loading rates ranging from 0.018 mm/s (quasi-static) to 740 mm/s (impact) were analyzed. Based on the test results and data analyses, the following conclusions were drawn.

1. The order of rate sensitivity on the single-fiber pull-out resistance in terms of the bond strength and pull-out energy was as follows: straight fiber > twisted fiber > hooked fiber.
2. The bundled straight steel fibers in UHPC effectively increased the pullout resistance at the impact loads compared to the static loads. The bond strength and pullout energy absorption capacity of multiple straight fibers were improved with an increase in the loading rate, but were not influenced by fiber spacing under the static or impact loading conditions.
3. The static pullout resistance of multiple hooked steel fibers in UHPC was improved by decreasing the fiber spacing, whereas the pullout resistance under the impact loads deteriorated with a closer spacing owing to the premature and severe matrix damage.
4. There was no clear improvement in the average bond strength of multiple twisted fiber cases as the loading rate and fiber spacing increased. On the other hand, the average bond strengths of single and bundled twisted fiber specimens were noticeably improved with increasing loading rate.
5. For the twisted and hooked fiber specimens, if the fiber ruptured or severe matrix spalling was generated, poorer pullout energy and equivalent bond strength were observed. Thus, UHPFRC composites need to be carefully designed to prevent fiber rupture and severe matrix damage to achieve an excellent post-cracking tensile performance at the impact loads.
6. The highest rate sensitivity of pullout resistance was obtained with the bundled fiber specimens regardless of the fiber type. Thus, the fiber bundles enhance the dynamic pullout resistances of both straight and deformed steel fibers in UHPC effectively. The highest DIF values of the bundled straight, hooked, and twisted

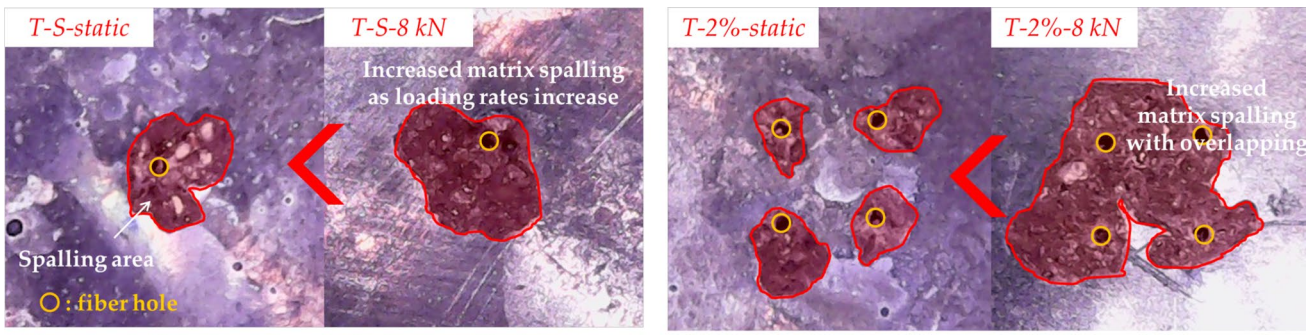

Fig. 16 Matrix spalling increase of twisted fiber according to loading rate: **a** single-fiber specimen and **b** multiple-fiber specimen

fibers in UHPC were found to be about 3.78, 1.57, and 1.41, respectively, at the impact loading conditions.

If two or more variables such as fiber geometry, fiber spacing, and pullout loading rates are applied in combination, test results showed unpredictable tendencies, even to be opposite. These results imply that it is very difficult to predict the tensile behavior of UHPFRC by using a single-fiber pullout test result for each single variable. Future research is needed to increase the correlation between pullout behavior of fibers and tensile behavior of UHPFRC to enable more accurate prediction of behavior of UHPFRC.

Acknowledgements This research was supported by a Grant (19CTAP-C152069-01) from Technology Advancement Research Program funded by Ministry of Land, Infrastructure and Transport of Korean Government.

Compliance with ethical standards

Conflict of interest The authors declared that they have no conflict of interest.

Ethical statement This research was done according to ethical standards.

References

1. Richard P, Cheyrezy M. Composition of reactive powder concretes. Cem Concr Res. 1995;25(7):1501–11.
2. Spasojevic A. Structural implications of ultra-high performance fiber reinforced concrete in bridge design. EPFL, Ph.D. thesis. 2008.
3. Habel K, Gauvreau P. Response of ultra-high performance fiber reinforced concrete (UHPFRC) to impact and static loading. Cem Concr Res. 2008;30(10):938–46.
4. Shin HO, Yoon YS, Cook WD, Mitchell D. Effect of confinement on the axial load response of ultrahigh strength concrete columns. J Struct Eng. 2015;141(6):04014151.
5. Yoo DY, Kang ST, Yoon YS. Enhancing the flexural performance of ultra-high-performance concrete using long steel fibers. Compos Struct. 2016;147:220–30.
6. Graybeal BA, Baby F. Development of direct tension test method for ultra-high-performance fiber-reinforced concrete. ACI Mater J. 2013;110(2):177–86.
7. AFGC. Ultra high performance fibre-reinforced concretes. Interim Recommendations. AFGC Publication, Bagneux, France. 2013.
8. ACI Committee 239. Ultra-high performance concrete, ACI Fall Convention. Toronto, ON, Canada. 2012.
9. JSCE. Recommendations for design and construction of ultra-high strength fiber reinforced concrete structures (Draft). Japan Society of Civil Engineers, Tokyo, Japan. 2004.
10. KCI-M-12-003. Design recommendations for ultra-high performance concrete K-UHPC. Korea Concrete Institute (KCI), Seoul. 2012.
11. Shaanag MJ, Brincker R, Hansen W. Pullout behavior of steel fibers from cement-based composites. Cem Concr Res. 1997;27(6):925–36.
12. Lee Y, Kang ST, Kim JK. Pullout behavior of inclined steel fiber in an ultra-high strength cementitious matrix. Constr Build Mater. 2010;24(10):2030–41.
13. Wille K, Naaman AE. Pullout behavior of high-strength steel fibers embedded in ultra-high-performance concrete. ACI Mater J. 2012;109(4):479–87.
14. Wille K, Naaman AE. Effect of ultra-high-performance concrete on pullout behavior of high-strength brass-coated straight steel fibers. ACI Mater J. 2013;110(4):451–61.
15. Tai YS, El-Tawil S. High loading-rate pullout behavior of inclined deformed steel fibers embedded in ultra-high performance concrete. Constr Build Mater. 2017;148:204–18.
16. Tai YS, El-Tawil S, Chung TH. Performance of deformed steel fibers embedded in ultra-high performance concrete subjected to various pullout rates. Cem Concr Res. 2016;89:1–13.
17. Yoo DY, Park JJ, Kim SW. Fiber pullout behavior of HPFRCC: effects of matrix strength and fiber type. Compos Struct. 2017;174:263–76.
18. Chun B, Yoo DY. Hybrid effect of macro and micro steel fibers on the pullout and tensile behaviors of ultra-high-performance concrete. Compos B Eng. 2019;162:344–60.
19. Kim JJ, Yoo DY. Effects of fiber shape and distance on the pullout behavior of steel fibers embedded in ultra-high-performance concrete. Cement Concr Compos. 2019;103:213–23.
20. Lee NK, Koh KT, Kim MO, Ryu GS. Uncovering the role of micro silica in hydration of ultra-high performance concrete (UHPC). Cem Concr Res. 2018;104:68–79.
21. Yoo DY, Banthia N, Lee JY, Yoon YS. Effect of fiber geometric property on rate dependent flexural behavior of ultra-high-performance cementitious composite. Cement Concr Compos. 2018;86:57–71.
22. Park JJ, Kang ST, Koh KT, Kim SW. Influence of the ingredients on the compressive strength of UHPC as a fundamental study to optimize the mixing proportion. In: Proceeding of second international symposium on ultra high performance concrete, Kassel (2008). p. 105–12.
23. Aoude H, Dagenais FP, Burrell RP, Saatcioglu M. Behavior of ultra-high performance fiber reinforced concrete columns under blast loading. Int J Impact Eng. 2015;80:185–202.
24. Krauthammer T. Recent observations on design and analysis of protective structures. Eng Struct. 2017;149:78–90.
25. Yoo DY, Kim S. Comparative pullout behavior of half-hooked and commercial steel fibers embedded in UHPC under static and impact loads. Cement Concr Compos. 2019;97:89–106.
26. Pacios A, Ouyang C, Shah SP. Rate effect on interfacial response between fibres and matrix. Mater Struct. 1995;28(2):83–91.
27. Yoo DY, Kim JJ, Park JJ. Effect of fiber spacing on dynamic pullout behavior of multiple straight steel fibers in ultra-high-performance concrete. Constr Build Mater. 2019;210(20):461–72.
28. Feng J, Sun WW, Wanga XM, Shi XY. Mechanical analyses of hooked fiber pullout performance in ultra-high-performance concrete. Constr Build Mater. 2014;69:403–10.
29. Wille K, Xu M, El-Twail S, Naaman AE. Dynamic impact factors of strain hardening UHP-FRC under direct tensile loading at low strain rates. Mater Struct. 2016;49(4):1351–65.
30. Xu M, Wille K. Effect of loading rates on pullout behavior of high strength steel fibers embedded in ultra-high performance concrete. Cement Concr Compos. 2016;70:98–109.
31. Markovic I. High-performance hybrid-fibre concrete: development and utilization. Delft University of Technology, Ph.D. Thesis. 2006.
32. Wang S, Zhang MH, Quek ST. Effect of high strain rate loading on compressive behaviour of fibre-reinforced high-strength concrete. Mag Concr Res. 2011;63(11):813–27.